PROTEINS: Structure, Function, and Bioinformatics 56:310–321 (2004)

Free Energy Surfaces of β-Hairpin and α-Helical Peptides Generated by Replica Exchange Molecular Dynamics with the AGBNP Implicit Solvent Model

Anthony K. Felts, Yuichi Harano, Emilio Gallicchio, and Ronald M. Levy*
Department of Chemistry and Chemical Biology and BIOMAPS Institute for Quantitative Biology, Rutgers University, Wright-Rieman Laboratories, 610 Taylor Rd, Piscataway, New Jersey

ABSTRACT **We have studied the potential of mean force of two peptides, one known to adopt a β-hairpin and the other an α-helical conformation in solution. These peptides are, respectively, residues 41–56 of the C-terminus (GEWTYDDATKTFTVTE) of the B1 domain of protein G and the 13 residue C-peptide (KETAAAKFERQHM) of ribonuclease A. Extensive canonical ensemble sampling has been performed using a parallel replica exchange method. The effective potential employed in this work consists of the OPLS all-atom force field (OPLS-AA) and an analytical generalized Born (AGB) implicit solvent model including a novel nonpolar solvation free energy estimator (NP). An additional dielectric screening parameter has been incorporated into the AGBNP model. In the case of the β-hairpin, the nonpolar solvation free energy estimator provides the necessary effective interactions for the collapse of the hydrophobic core (W43, Y45, F52, and V54), which the more commonly used surface-area-dependent nonpolar model does not provide. For both the β-hairpin and the α-helix, increased dielectric screening reduces the stability of incorrectly formed salt bridges, which tend to disrupt the formation of the hairpin and helix, respectively. The fraction of β-hairpin and α-helix content we obtained using the AGBNP model agrees well with experimental results. The thermodynamic stability of the β-hairpin from protein G and the α-helical C-peptide from ribonuclease A as modeled with the OPLS-AA/AGBNP effective potential reflects the balance between the nonpolar effective potential terms, which drive compaction, and the polar and hydrogen bonding terms, which promote secondary structure formation. Proteins 2004;56:310–321.**

Key words: replica exchange method; β-hairpin; α-helix; implict solvent model; potential of mean force

INTRODUCTION

The protein folding problem is of fundamental importance in modern structural biology. Recent advances in experimental techniques have helped to elucidate thermodynamic and kinetic mechanisms that underlie different stages of the folding process.[1–6] Computer simulations performed at various levels of molecular detail have played a central role in the interpretation of experimental studies. Molecular simulations using models based on fully atomic representations are becoming more accurate and practical and are increasingly employed to simulate protein folding and predict protein structures.[7–15] Due to the large number of degrees of freedom, however, these simulations require extensive computer resources to obtain meaningful results, especially when the solvent environment is treated explicitly. Because of this, many recent computational studies have been carried out with implicit solvent models.[15–19] The question of how well implicit solvent effective potentials combined with detailed atomic protein models can predict thermodynamic and kinetic aspects of protein folding is under active investigation.[9,10,12,13,15,18–26]

Understanding the molecular basis for the thermodynamic stability and folding kinetics of typical secondary structural elements is a necessary step in the development of accurate protein folding models. The study of α-helical and β-sheet peptide fragments isolated from their protein environments has therefore been actively pursued.[1,4,27] Until the mid 1980s, linear peptides were believed to be poorly structured in water,[28,29] a view supported by theoretical models.[30,31] Several linear peptides that retain many structural features of full-size proteins have since been discovered.[27,32] The C-peptide of ribonuclease A has been found to retain a significant fraction of α-helical content in solution.[33,34] More recently, the C-terminal peptide of protein G has been shown to retain many features of its original β-hairpin structure in solution[35] and has been the subject of extensive studies, both experimental[35–40] and theoretical.[16–19,41–49] Due to their small size, peptides of this kind are particularly useful as target systems for analysis and refinement of molecular force fields.[50]

In early studies, it was not possible to analyze large enough regions of conformational space to offer meaning-

*Correspondence to: Ronald M. Levy, Department of Chemistry and Chemical Biology and BIOMAPS Institute for Quantitative Biology, Rutgers University, Wright-Rieman Laboratories, 610 Taylor Rd, Piscataway, NJ 08854-8087. E-mail: ronlevy@lutece-rutgers.edu

Received 11 November 2003; Revised 18 December 2003; Accepted 5 January 2004

Published online 14 May 2004 in Wiley InterScience (www.interscience.wiley.com). DOI: 10.1002/prot.20104

ful comparisons between the thermodynamic predictions of different force field models concerning the propensities of various peptides to form either α-helical or β-hairpin conformations. Recent advances in parallel sampling techniques[50–52] and the widespread availability of large numbers of processors have now made possible the calculation of the full potential of mean force of small-to-medium sized peptides in solution.[15,18,46,47,50] Schaefer and coworkers have studied the stability of two designed sequences corresponding to α-helical and β-hairpin conformations in implicit solvent using adaptive umbrella sampling.[53] We are not aware of any studies of all-atom effective potentials with implicit solvation that analyze the free energy surface for *both* α-helical and β-hairpin peptides using unbiased Boltzman sampling. In this article, we construct the potentials of mean force of various models of the C-terminal peptide of protein G and the C-peptide of ribonuclease A in solution using the OPLS all-atom (AA) force field[54,55] with the AGBNP implicit solvent model[26] and compare these predictions with experimental and other theoretical results.

The stability of the β-hairpin-forming C-terminal peptide (residues 41–56) of the B1 domain of protein G[56] was first demonstrated by Blanco and coworkers by nuclear magnetic resonance (NMR).[35] (It has been suggested that this β-hairpin is the folding nucleus of the B1 domain.[36,40]) Based on the NMR measurements, Blanco et al. determined that the population of the β-hairpin was around 42% at 278K.[35] Kinetic experiments were performed on this peptide by Muñoz et al. by following the flourescence of W43 after nanosecond laser temperature jumps. They measured the change in flourescence as W43 was buried into the hydrophobic core consisting of the residues W43, Y45, F52, and V54. They found a β-hairpin population of ~80% at 273K;[37] Roccatano et al. pointed out that this population corresponds to the fraction of structures that have a collapsed hydrophobic core rather than the fraction of native β-hairpin structures.[44] Muñoz et al. proposed a zipper-like mechanism for the folding, where the β-turn folds first, followed by the sequential formation of β-sheet hydrogen bonds starting from the turn and proceeding towards the termini of the peptide, bringing the hydrophobic core together.[37,38] Honda et al.[39] and Kobayashi et al.[40] performed temperature-dependent NMR experiments to study the thermodynamics of folding of the β-hairpin of protein G. They proposed a cooperative folding mechanism in which the collapse of the hydrophobic core and formation of the β-sheet hydrogen bonds occur simultaneously.[39,40]

There have been several computational studies of the C-terminal β-hairpin of protein G. Some have used reduced models to simulate the peptide, while others have treated the peptide in full atomic detail in both explicit and implicit solvent. Kolinski et al. studied the ensemble of conformations of this peptide using a lattice model.[41] Zhou and Linhananta performed MD simulations using a square-well potential for the non-bonded interactions in the absence of electrostatics and solvent environment.[42] Several groups have carried out molecular dynamics (MD) simulations of the C-terminal peptide of protein G using all-atom models in explicit solvent.[43–49,57] The studies of García and Sanbonmatsu[46] and Zhou et al.[47] were carried out using the parallel replica exchange sampling method (REM). (In both studies, capping groups were placed on the termini of the polypeptide, disrupting salt bridge formation between the termini.) The free energy surfaces they constructed serve as benchmarks for our current studies with the AGBNP implicit solvent potential. Explicit solvent simulations have highlighted the importance of the collapse of the hydrophobic core for the folding of the β-hairpin.[43–49,57] Ma and Nussinov replaced the backbone hydrogens with flourine atoms to destroy the hydrogen-bonding network between the two strands. They found that the hydrophobic core provides enough stabilization to maintain the β-hairpin despite the repulsion between the flourines and carboxyl oxygens.[45] Another factor that has been reported to contribute to the stability of the β-hairpin is salt bridges; one formed between the peptide terminal residues[49] and another in the turn region of the hairpin.[45,49]

The C-terminal peptide of protein G has been simulated using implicit solvent by several groups. Dinner et al. studied the peptide using the EEF1 implicit solvent model[58] and estimated a β-sheet population of 54% at 280K[16] in reasonable agreement with experimental data.[35] Zagrovic et al. studied the capped peptide using the generalized Born/surface area (GB/SA) implicit solvent model[59] and ensemble molecular dynamics to simulate folding. They estimated the potential of mean force (PMF) based on those trajectories that folded,[17] but this overestimates the stability of the β-hairpin. Zhou and Berne[18] employed the surface generalized Born (SGB) implicit solvent model[60] and constructed the PMF for the peptide using replica exchange sampling. They observed that the PMF in implicit solvent did not agree with the PMF they previously reported for the β-hairpin based on simulations in explicit solvent. The β-hairpin was not stable at room temperature using the SGB implicit solvent model. They attributed this result in part to the formation of salt bridges, especially the one between K50 and E56, which prevents the formation of the hydrophobic core. They suggest that this salt bridge is allowed to form because of insufficient screening of the electrostatic interactions in the SGB model.[18] Zhou has continued to study the β-hairpin using the GB/SA implicit solvent model[59] with various AMBER all-atom force fields.[61]

Other peptides that form β-hairpins and small β-sheets have been studied using both explicit and implicit solvent models. Ma and Nussinov[62] studied the peptide YITNSDGTWT, which was designed by de Alba et al.[63] to form a β-hairpin. They noted that the continuum solvent model based on solving the Poisson–Boltzman equation with a surface area term for the nonpolar solvation energy was not able to properly discriminate the native fold from misfolded conformations. They corrected their model, using a surface area term divided into polar and nonpolar contributions and adding a term for the vibrational entropy.[62] Bursulaya and Brooks[10] report the PMF for the

20-residue designed peptide Betanova which forms a small three-strand β-sheet in both explicit (using TIP3P water model) and implicit (using GB) solvent. They reported qualitative agreement in the free energy surface between the two solvent treatments.[10]

The α-helical peptide studied in this work is the C-peptide (KETAAAKFERQHM), a fragment of ribonuclease A, consisting of residues 1 through 13. The helical nature of the C-peptide was first observed by circular dichrosim (CD) by Brown and Klee.[64] This peptide was further studied by CD and NMR measurements by the Baldwin group.[33,34] They noted the formation of a salt bridge between residues E2 and R10. NOE measurements were made on an analogue of the C-peptide by Osterhout et al.[65] A considerable amount of theoretical work on the C-peptide has been carried out by the Okamoto group.[66–69] They studied the C-peptide using multicanonical Monte Carlo (MC) simulations with a distance-dependent dielectric function to account for solvation effects.[66,67] A more molecular treatment of implicit solvation was used in MC simulated annealing studies; RISM theory was applied to model the solvation.[68] The replica exchange method has been applied by this group to another α-helical peptide, the 17-residue fragment from ribonuclease T1 using a distance dielectric function to treat solvation effects.[70]

A few recent papers have reported the results of simulations of both α-helix and β-hairpin secondary structure motifs with various models of solvation. The different treatments of solvation have included distance-dependent dielectric functions,[69] GB implicit solvent models,[12,53] and simulations in explicit water solvent.[71] None of these studies have examined how well these effective potential functions reproduce the free energy surface of both α-helical and β-hairpin secondary structure. In this work, we employ the OPLS-AA force field[54,55] and the recently developed implicit solvation model (AGBNP)[26] to simulate the free energy surface of the C-peptide of ribonuclease A and the C-terminus of the B1 domain of protein G. The AGBNP implicit solvent model is based on a novel pairwise descreening implementation of the generalized Born model.[59] AGBNP makes use of a new, parameter-free algorithm to calculate the scaling coefficients used in the pairwise descreening scheme to take into account atomic overlaps. The AGBNP model also includes a novel nonpolar solvation free energy estimator which consists of two separate terms, a cavity formation term and a term that corresponds to the van der Waals attraction between the solute and solvent.[26] The nonpolar model was developed in light of limitations of the standard solvent-accessible surface-area model for proteins, which are more apparent at higher resolution.[72] The complete effective potential function we used in this study is referred to as the OPLS-AA/AGBNP potential. Also included in the AGBNP model is an additional electrostatic screening parameter, which effectively increases the dielectric screening around atomic groups with formal charges and which we have used to correct for any overestimation of salt bridge formation. We explore the free energy surfaces of the two peptides using a parallel REM combined with a MD algorithm.[51] The OPLS-AA/AGBNP potential was found to be capable of predicting the correct, thermodynamically stable states of these two peptides.

MATERIALS AND METHODS

The MD replica exchange canonical sampling method has been implemented in the molecular simulation package IMPACT following the approach proposed by Sugita and Okamoto.[51] In this method, a series of structures (the replicas) are simulated in parallel using MD at different temperatures. The temperatures, T_m and T_n, of two replicas, i and j, respectively, are exchanged with the following Metropolis transition probability:[51]

$$W\{(T_m, T_n\} \rightarrow \{T_n, T_m\}) = \begin{cases} 1 & \text{for } \Delta \leq 0 \\ \exp(-\Delta) & \text{for } \Delta > 0 \end{cases} \quad (1)$$

where

$$\Delta \equiv (\beta_n - \beta_m)(E_i - E_j), \quad (2)$$

β_m is equal to $1/kT_m$ and E_i is the current potential energy of replica i (and similarly for β_n and E_j). After the exchange, the velocities of replicas i and j were resampled at the new temperatures. In our simulations, 20 replicas were run in parallel at the following temperatures (in K): 270, 283, 298, 313, 328, 345, 363, 381, 400, 421, 442, 465, 488, 513, 539, 566, 594, 625, 656, and 690. Each replica was thermalized at its respective temperature for 100 ps with a timestep of 1 fs. MD replica exchange sampling was carried out for a total of 4 ns using a timestep of 1 fs. Transitions between adjacent temperatures were attempted every 100 MD steps. The transition acceptance ratio we obtained was around 40%.

Immediately prior to attempting temperature exchanges, the configuration of each replica was stored for later analysis. For each 1 ns time window of sampling, we calculated the PMF for some state, X, using the following relationship:

$$\mathrm{PMF}(X) = -RT \log P(X), \quad (3)$$

where $P(X)$ is the normalized probability of being in state X. We examined how the PMF changed from one time window to the next. The system was considered to be equilibrated when the PMF did not change appreciably from one time window to the next; an initial run of 2 ns was found to be required for equilibration. We used the last 2 ns of the 4 ns trajectories to generate the free energy surfaces; therefore, there were 20,000 configurations at each temperature that were used to construct the final potentials of mean force for the β-hairpin and α-helical peptides.

MD simulations were carried out using the OPLS-AA force field and the AGBNP implicit solvent model, which is based on a novel pairwise descreening implementation[26] of the generalized Born model,[59] and a recently proposed non-polar hydration free energy estimator described below.[26] AGBNP employs a parameter-free and conformation-dependent analytical scheme to obtain the pairwise descreening scaling coefficients used in the computation of

the Born radii. The agreement between the AGBNP Born radii and exact numerical calculations was found to be excellent. The AGBNP nonpolar model consists of an estimator for the solute–solvent van der Waals interaction energy in addition to an analytical surface area component corresponding to the work of cavity formation.[26] Because AGBNP is fully analytical with first derivatives it is well suited for MD sampling. A detailed description of the AGBNP model and its implementation is provided in ref. 26.

For this study, we also used a modified generalized Born pair function f_{ij} designed so that the dielectric screening between particular atom pairs could be adjusted. In the standard implementation of the GB model, the electrostatic component of the hydration free energy is estimated as

$$\Delta G_{\text{elec}} \simeq \Delta G_{\text{GB}} = \Delta G_{\text{self}} + \Delta G_{\text{pair}} \tag{4}$$

where

$$\Delta G_{\text{self}} = -\frac{1}{2}\left(\frac{1}{\epsilon_{\text{in}}} - \frac{1}{\epsilon_{\text{w}}}\right)\sum_i \frac{q_i^2}{B_i} \tag{5}$$

is the sum of the atomic GB self-energies, and

$$\Delta G_{\text{pair}} = -\left(\frac{1}{\epsilon_{\text{in}}} - \frac{1}{\epsilon_{\text{w}}}\right)\sum_{i<j} \frac{q_i q_j}{f_{ij}} \tag{6}$$

is the sum of the GB pair-energies. In eqs. (5) and (6), ϵ_{in} is the dielectric constant of the interior of the solute and ϵ_{w} is the dielectric constant of the solvent, q_i is the partial charge of atom i, B_i is the Born radius of atom i. The inverse of the Born radius for atom i is given by the integral of $1/r^4$, centered on atom i, over the solvent region,

$$\frac{1}{B_i} = \frac{1}{4\pi}\int_{\text{Solvent}} d^3\mathbf{r}\,\frac{1}{(\mathbf{r}-\mathbf{r}_i)^4} \tag{7}$$

and

$$f_{ij} = \sqrt{r_{ij}^2 + B_{ij}^2 \exp(-r_{ij}^2/4B_{ij}^2)} \tag{8}$$

where r_{ij} is the distance between atoms i and j, $B_{ij} = \sqrt{B_i B_j}$ is the geometric average of the Born radii of atoms i and j.

We introduce a modified GB pair function

$$f_{ij} = \sqrt{r_{ij}^2 + S_{ij}^2 B_{ij}^2 \exp(-r_{ij}^2/4B_{ij}^2)} \tag{9}$$

which differs from the original expression [eq. (8)] by the presence of the parameter S_{ij}. S_{ij} is defined as the geometric average, $\sqrt{S_i S_j}$, of the screening constants, S_i and S_j, assigned to atoms i and j. The screening constants are nonnegative, dimensionless parameters. The original GB pair interaction energy is recovered when the screening constants of both atoms are equal to 1. Note that because the modified GB pair function [eq. (9)] does not reduce to B_{ij} at zero interatomic distance, the corresponding GB energy does not reproduce the Born limit in the case of complete atomic overlap. This has a negligible effect on the relative energies analyzed in this study because bond lengths vary little from one conformation to another, whereas the distance between non-bonded atom pairs is well beyond the overlap distance. The effect of the S_{ij} parameter can be rationalized in terms of the GB pair effective dielectric function $\epsilon_{ij}(r_{ij})$[21] defined by the identity

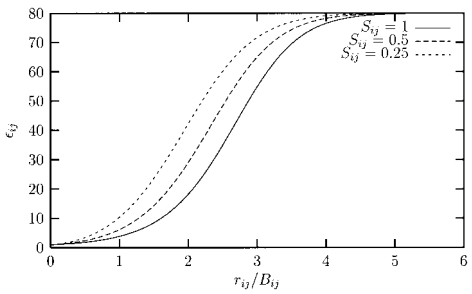

Fig. 1. The generalized Born effective pair dielectric function for various values of the screening parameter, S_{ij}. The effective pair dielectric function, ϵ_{ij}, from eq. (11), is plotted with respect to the ratio of the distance between atoms i and j, r_{ij}, and the pair Born radius, B_{ij}.

$$\frac{q_i q_j}{\epsilon_{ij}(r_{ij}) r_{ij}} = \frac{q_i q_j}{\epsilon_{\text{in}} r_{ij}} - \left(\frac{1}{\epsilon_{\text{in}}} - \frac{1}{\epsilon_{\text{w}}}\right)\frac{q_i q_j}{f_{ij}} \tag{10}$$

which yields

$$\frac{1}{\epsilon_{ij}(r_{ij})} = \frac{1}{\epsilon_{\text{in}}} - \left(\frac{1}{\epsilon_{\text{in}}} - \frac{1}{\epsilon_{\text{w}}}\right)\left[1 + \frac{S_{ij}^2}{x_{ij}^2}\exp(-x_{ij}^2/4)\right]^{-1/2} \tag{11}$$

where

$$x_{ij} = \frac{r_{ij}}{B_{ij}} \tag{12}$$

Another approach to correct the dielectric screening in the GB model has been carried out by Case and coworkers[21,73] to account for salt effects. They present a modification of the prefactor of interior and exterior dielectric constants to adjust the dielectric screening.[21,73]

Figure 1 shows the effective dielectric function for $\epsilon_{\text{w}} = 80$ and for various values of screening parameter S_{ij}. The effective dielectric function has a limiting value of 1 for distances r_{ij} much smaller than the pair Born radius B_{ij} and reaches a maximum value of 80 for r_{ij} values much larger than B_{ij}. The parameter S_{ij} regulates the value of the effective dielectric at intermediate distances. The smaller the value of S_{ij}, the larger the effective dielectric constant at a given distance. For instance, for $r_{ij} = 2B_{ij}$ the value of the effective dielectric with $S_{ij} = 0.25$ is roughly twice the value of the effective dielectric with $S_{ij} = 1$.

In some of the calcuations in this work, we assigned a screening constant of 0.5 to the oxygen atoms of the carboxylate groups of the glutamate and aspartate residues and to the nitrogen atoms of the ammonium and guanadinium groups of the lysine and arginine residues. The screening constant for all other atoms was set to 1. In this way, the screening parameter S_{ij} for interactions involving two highly charged atoms (the oxygen and nitrogen atoms of charged residues) had a value of 0.25, the screening parameter for interactions between a highly

charged atom and an atom without a formal charge was 0.5 and the screening parameter for all other interactions remained at the standard value of 1. Our work with protein decoys[14] and the work of others on side chain and loop modelling[74–76] indicate that salt bridge formation is overestimated by generalized Born solvation models. The additional dielectric screening was designed to reduce the occurrence of salt bridges between oppositely charged residues as well as to decrease the repulsion between like-charged residues in some of the peptide simulations described below. Free energy surfaces for the peptides generated with and without the additional dielectric screening are compared.

The nonpolar solvation free energy is given by the sum of two terms, the free energy to form the cavity in solvent filled by the solute and the dispersion attraction between solute and solvent. The nonpolar free energy is written as[26]

$$\Delta G_{np} = \sum_i (\gamma_i A_i + \Delta G_{\mathrm{vdW}}^{(i)}) \tag{13}$$

where the first term is the cavity term, γ_i is the surface tension proportionality constant for atom i, and A_i is the solvent exposed surface area of atom i. The second term is the dispersion interaction term which is given by[26]

$$\Delta G_{\mathrm{vdW}}^{(i)} = \alpha_i \frac{-16\pi\rho_w\epsilon_{i,w}\sigma_{i,w}^6}{3(B_i + R_w)^3}, \tag{14}$$

where α_i is an adjustable solute–solvent van der Waals dispersion parameter for atom i. The parameter ρ_w is the number density of water at standard conditions (0.033428/Å^3). The values of $\epsilon_{i,w}$ and $\sigma_{i,w}$ are the pairwise Lennard-Jones (LJ) well-depth and diameter parameters for atom i and the TIP4P water oxygen as given by the OPLS-AA force field.[54,55] ($\epsilon_{i,w} = \sqrt{\epsilon_i \epsilon_w}$, where ϵ_i is the LJ well-depth for atom i and ϵ_w is a similar value for the TIP4P water oxygen. The ϵ for water hydrogens is set to zero. $\sigma_{i,w}$ is defined in a similar manner.) R_w is the radius of a water molecule (1.4 Å). By not incorporating the Lennard-Jones parameters into the dispersion parameter, α_i, atoms with different though similar ϵ_i and σ_i values are assigned the same α so as to minimize the number of adjustable parameters. B_i is the Born radius of atom i. The Born radius in this equation provides a measure of how buried atom i is in the solute. The deeper the atom is in the solute, the smaller its contribution to the total solute–solvent dispersion interaction energy. The form of eq. (14) for the solute–solvent van der Waals interaction energy component has been derived on the basis of simple physical arguments.[26] In this work we use the same parameterization of α and γ as in the work of Gallicchio and Levy.[26]

RESULTS AND DISCUSSION

The Capped C-Terminal Polypeptide From Protein G

In order to compare our results with the explicit solvent results of García and Sanbonmatsu[46] and Zhou et al.[47] who studied the capped form of the peptide, we first investigated the potential of mean force of the capped C-terminal peptide from the B1 domain of protein G (sequence: G41EWTYDDATKTFTVTE56). The peptide, which was shown to form a β-hairpin,[35] is capped with acetyl (Ace) and N-methyl amide (Nme) groups at the N- and C-termini, respectively. We constructed the potential of mean force from replica exchange simulations with various solvation models, as shown in Figures 2–4. Figure 2 shows the free energy surface generated using the OPLS-AA/AGBNP potential with a surface-area-dependent nonpolar model and with the default level of dielectric screening (S_i is set to 1 for all atoms). In this model, the nonpolar solvation free energy is simply proportional to the solute surface area, as commonly used in standard implementations of generalized Born models such as SGB[60]

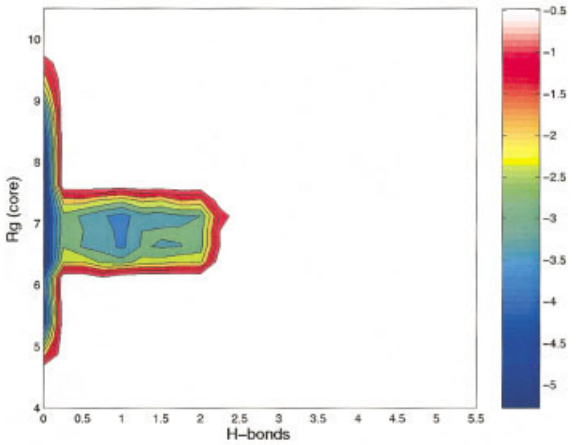

Fig. 2. The potential of mean force of the capped C-terminal peptide from protein G with respect to number of native hydrogen bonds ('H bonds') and radius of gyration ('Rg(core)' in Å) of hydrophobic core consisting of W43, Y45, F52, & V54. The OPLS-AA/AGBNP potential was used with the default dielectric screening (S_i = 1.0 was all atoms). A simple surface-area-dependent model for the nonpolar solvation energy was used (γ = 15 cal/mol/Å^2). The temperature was 313K. The polypeptide was capped with Ace and Nme groups. The energy is in units of kcal/mol.

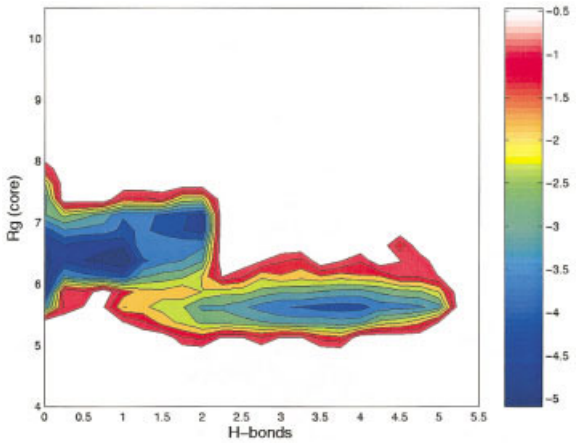

Fig. 3. See caption in Figure 2 for details. The OPLS-AA/AGBNP potential was used with the full nonpolar model and with the default dielectric screening.

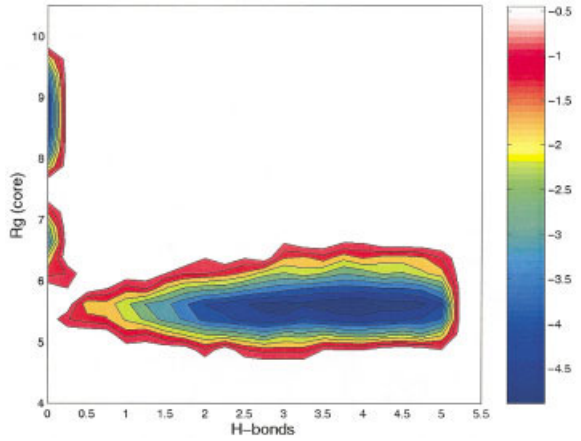

Fig. 4. See the caption of Figure 2 for details. The OPLS-AA/AGBNP potential was used with the full nonpolar model and with additional dielectric screening of charged side chains (S_{ij} = 0.5 for atoms with formal charges).

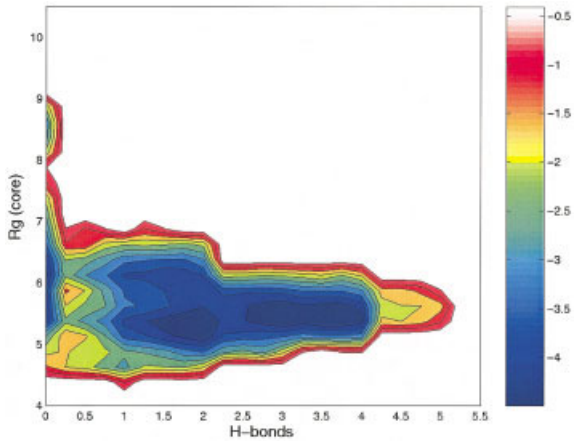

Fig. 5. The potential of mean force of the uncapped zwitterion form of the C-terminal peptide from protein G. See the caption to Figure 2 for details. The OPLS-AA/AGBNP potential was used with the full nonpolar model and with the default dielectric screening (S_{ij} = 1.0 for all atoms).

and GB/SA.[59] The surface tension parameter, γ, is set to 15 cal/mol/Å^2. The OPLS-AA/AGBNP potential with this surface area nonpolar model roughly corresponds to the OPLS-AA/SGB potential used in the studies by Zhou and Berne.[18] Figure 3 shows the free energy surface generated using the OPLS-AA/AGBNP potential with the full nonpolar function [eq. (13)] and default dielectric screening (S_i = 1 for all atoms). Finally, Figure 4 shows the free energy surface generated with the OPLS-AA/AGBNP potential, including the full nonpolar function [eq. (13)] and increased dielectric screening of charged side chains (S_i is set to 0.5 for atoms with formal charges). The free energy surfaces shown in Figures 2–4 are plotted with respect to the radius of gyration of the hydrophobic core side chains (residues W43, Y45, F52, and V54) and the number of native β-sheet hydrogen bonds. A hydrogen bond is defined to have formed when the distance between the amide N and carboxyl O is within 3.5 Å and the angle between the N—H and O—C bonds is larger than 150°. The potential of mean force obtained using the full nonpolar function and additional dielectric screening of charged sidechains shown in Figure 4 is similar to the results with explicit solvent of García and Sanbonmatsu[46] and Zhou et al.,[47] except for the appearance of a free energy barrier separating the unfolded and collapsed states. Below we discuss the various effects that the nonpolar and dielectric screening parameters have on the potential of mean force.

Effects of Nonpolar Parameters

The influence of the nonpolar parameters on the free energy surface of the peptide was demonstrated by comparing the potential of mean force of the capped peptide obtained using the solute surface area nonpolar model (Fig. 2) to the free energy surfaces shown in Figures 3 and 4 obtained with the full nonpolar function [eqs. (13) and (14)]. When using the surface-area-only model for the nonpolar interactions, the hydrophobic core (W43, Y45, F52, and V54) does not collapse to the same extent as it

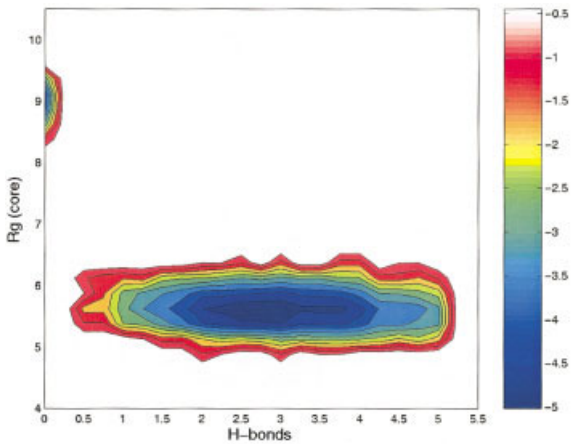

Fig. 6. Same as Figure 5 except the OPLS-AA/AGBNP potential was used with additional dielectric screening of charged side chains (S_{ij} = 0.5 for atoms with formal charges).

does in structures generated with the full nonpolar function (compare Fig. 2 to Figs. 3 and 4). At 270K, only 12.8% of the structures generated with the surface area nonpolar model have a collapsed hydrophobic core (a conformation is said to have a collapsed hydrophobic core when its radius of gyration of the side chains of residues W43, Y45, F52, and V54 is less than 6 Å). In Figure 2 it can be clearly seen that little population is found below a hydrophobic core radius of gyration of 6 Å. When the full nonpolar function of the OPLS-AA/AGBNP potential is used, the percentage of hydrophobic collapse increases to 37.8% with the default dielectric screening (Fig. 3) and 94.1% with the increased dielectric screening of charged side chains (Fig. 4).

The decreased degree of hydrophobic collapse with the full nonpolar function and the default dielectric screening (Fig. 3) compared to that with additional dielectric screening (Fig. 4) is due to a salt bridge forming between

Fig. 7. The C_α trace of the backbone of a fully formed β-hairpin of the uncapped peptide is shown above. The structure corresponds to one from the ensemble generated with the OPLS-AA/AGBNP potential using additional dielectric screening. The temperature was 313K.

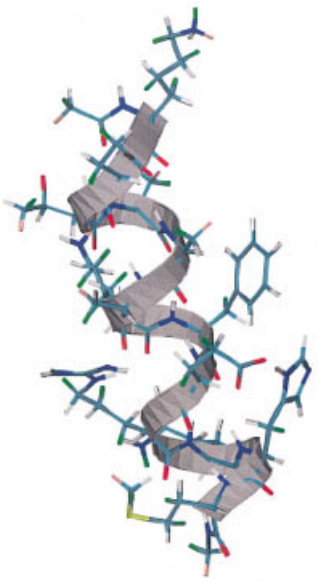

Fig. 8. The structure of the helical form of the C-peptide. The backbone atoms are traced with a ribbon model. The structure corresponds to a snapshot from the ensemble generated using the OPLS-AA/AGBNP potential with additional dielectric screening ($S_i = 0.5$ for charged atoms).

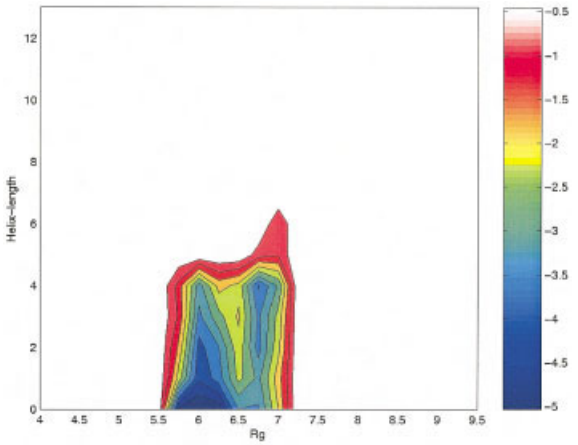

Fig. 9. The free energy contour map of C-peptide with respect to helical structure ('Helix-length') and radius of gyration ('Rg,' in Å). The potential is OPLS-AA/AGBNP with full nonpolar function and with default dielectric screening (S_i for all atoms). The temperature was 313K. The energy is in units of kcal/mol.

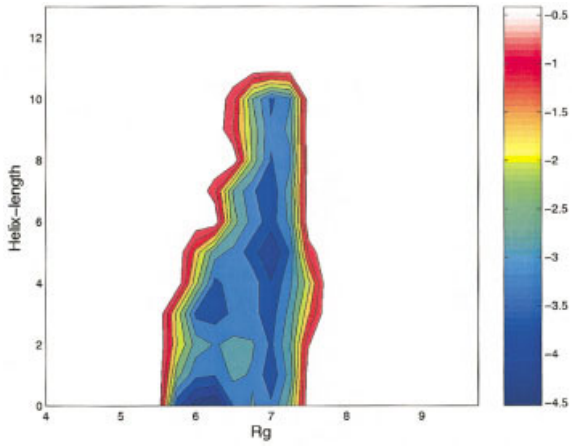

Fig. 10. See the caption to Figure 9. The OPLS-AA/AGBNP potential was used with the full nonpolar function and with additional dielectric screening of charged side chains ($S_i = 0.5$ for charged atoms).

the side chains of K50 and E56 that hinders the formation of the hydrophobic core. The structures with this salt bridge contribute to the deep minimum in the potential of mean force around zero hydrogen bonds shown in Figure 3. The same salt bridge also predominately appears in the structures generated using the OPLS-AA/AGBNP potential with the surface area nonpolar model, as seen in the deep minimum at zero hydrogen bonds in Figure 2. (This potential is similar to the OPLS-AA/SGB potential used by Zhou and Berne.[18] They also observed the salt bridge between residues K50 and E56 and noted that it prevents the formation of the β-hairpin.) However, significantly more of the structures generated with the full AGBNP nonpolar function have a collapsed hydrophobic core compared to those generated with the surface area nonpolar model. The full nonpolar model of the OPLS-AA/AGBNP potential favors the formation of the collapsed hydrophobic core of the peptide even in the presence of the destructive salt bridge between residues K50 and E56.

Effects of Salt Bridges and Dielectric Screening

As already mentioned, in the absence of additional dielectric screening, the formation of a salt bridge between residues K50 and E56 destabilizes the hydrophobic core. Increased dielectric screening of charged side chains aids in β-hairpin formation by reducing the interaction between charged atom pairs, which otherwise couple to create unfavorable salt bridges. This is demonstrated by comparing the relative populations of the β-hairpin conformation obtained with and without the additional dielectric screening of the charged side chains, as shown in Figures 4 and 3, respectively. The β-hairpin population is defined as the fraction of native β-sheet hydrogen bonds in the ensemble relative to the maximum number possible. At 283K, the relative population of the β-hairpin was 10% with the default dielectric screening. With additional dielectric screening, the relative β-hairpin population increased to 51%.

With the default dielectric screening, essentially all of the structures contain salt bridges at 298K, whereas only 43% of the structures contain salt bridges when additional dielectric screening of charged side chains is introduced. The free energy for forming any salt bridge in the presence of additional dielectric screening is 0.09 kcal/mol at 298K, indicating that the salt bridge is slightly disfavored. With increased dielectric screening, the percentage of structures with salt bridges is comparable to the value observed in the explicit solvent study by Roccatano et al. (36% at 300K).[44] The dominant salt bridge of the capped peptides forms between residues D47 and K50 along the turn region of the hairpin. It has been noted by Tsai and Levitt in their explicit solvent calculations that this salt bridge can stabilize the β-hairpin.[49] In contrast, Zhou states that the formation of this salt bridge is "erroneous."[19] Our results show that this salt bridge can be present without disrupting the β-hairpin conformation.

Uncapped C-Terminal Polypeptide from Protein G

While previous replica exchange simulations of the C-terminal polypeptide from the B1 domain of protein G in explicit and implicit solvent have been carried out using the capped peptide,[18,19,46,47] the experiments have been performed on the zwitterion form of the peptide (i.e., the uncapped peptide).[35–38] We investigated the effect of capping on the potential of mean force of this peptide by comparing the above results for the capped peptide to those for the uncapped peptide. We performed simulations on the uncapped peptide with the OPLS-AA/AGBNP effective potential, including the full nonpolar function, both with and without additional dielectric screening of charged sidechains. The results are shown in Figure 5 (default dielectric screening) and in Figure 6 (additional dielectric screening).

A salt bridge between the N- and C-termini can form in the uncapped polypeptide but cannot form in the capped peptide. As can be seen by comparing Figure 3 to Figure 5, with the default dielectric screening, the β-hairpin population of the uncapped peptide (26%) is significantly larger than the β-hairpin population of the capped peptide (10%) with the same solvation model. This is due to the stabilizing effects of the salt bridge between the N- and C-termini. The terminal salt bridge compensates for the disruptive interaction between the charged residues of K50 and E56, which form a salt bridge, preventing the formation of the hairpin. The salt bridge between K50 and E56 is found in many of the structures of the zwitterion generated without additional dielectric screening; these correspond to the population of structures found with zero native β-sheet hydrogen bonds (see Fig. 5). The population of this disruptive salt bridge is reduced when increased dielectric screening of the charged side chains is applied, and consequently the β-hairpin population is increased from 26% to 40% (compare Figs. 5 and 6). The predicted β-hairpin population of the uncapped peptide agrees well with the experimental results of Blanco et al. (42% at 283K)[35] carried out on the same uncapped system. The degree of hydrophobic collapse (98%) agrees reasonably well with the experimental results reported by Muñoz et al. who observed around 80% hydrophobic collapse at 270K.[37]

Shown in Figure 7 is a C_α trace of the backbone of a completely formed β-hairpin representative structure (hydrophobic core radius of gyration of 5.4 Å and five native hydrogen bonds). This structure was generated with the OPLS-AA/AGBNP effective potential with additional dielectric screening of charged side chains. As can be seen in this figure, the β-hairpin adopts a right-handed twist along the β-strands. The right-handed twisting of this β-hairpin, which is a generally observed characteristic of β-sheets,[77–80] was also observed in the explicit solvent simulations of Roccatano et al.[44]

Folding Mechanism of the β-Hairpin

The replica exchange simulations provide thermodynamic information but cannot directly give details about folding kinetics. However, we can infer something about the mechanism of folding of the β-hairpin from the changes in various structural parameters over the different temperatures used during the replica exchange simulations. In particular, we examined the variations with temperature of the fraction of hydrophobic collapse, the fraction of β-hairpin hydrogen bonds, and the fraction of folded β-turns. We observed that the collapse of the hydrophobic core and the formation of the β-sheet hydrogen bonds and β-turn occur at roughly the same temperature. This suggests that the folding of the β-hairpin is a cooperative process that involves the simultaneous formation of the hydrophobic core, the hydrogen bonds, and β-turn. This is consistent with the experimental results of Honda et al.[39] and Kobayashi et al.[40] who also observed, through temperature-dependent NMR experiments, a cooperative mechanism in which the collapse of the hydrophobic core and formation of hydrogen bonds occur simultaneously. Theoretical simulations of the kinetics of the peptide indicate that the hydrophobic core collapses first, followed by the formation of the hydrogen bonds.[43,57] The recent results of Bolhuis suggests that the intermediate state, consisting of a packed hydrophobic core and no secondary structure, is very transient, yielding a two-state mechanism between the unfolded and folded states.[57] While the replica exchange sampling method does not allow us to infer kinetics directly, the ensemble of structures generated at various temperatures can be used to explore the mechanism of β-hairpin formation. Further studies of this are underway in our lab. We should point out, however, that since the generalized Born model has not been properly parameterized for high temperatures, we observed transition temperatures for the formation of the β-hairpin that were artificially high, ~485K. Additional analysis of temperature dependence will be reported elsewhere.

C-Peptide of Ribonuclease A

We carried out replica exchange MD simulations of a thirteen-residue fragment from ribonuclease A, which forms an α-helix in solution. There are many peptides reported to adopt a mostly α-helical conformation without aggregation in various solvent conditions.[81] Alanine is

commonly known to be a helix-forming residue in proteins; therefore, many synthesized α-helical peptides are based on alanine. We studied a naturally occurring sequence, the C-peptide of ribonuclease A (Fig. 8), which forms an α-helix in aqueous solution even when isolated from the original protein.[64] The C-peptide has been well studied both experimentally[33,34,65] and theoretically.[66–69] In this study, the 13-residue peptide was capped with the normal acetyl (Ace) and N-methyl amide (Nme) groups, resulting in the blocked peptide sequence of Ace-KETAAAKFER-QHM-Nme.

Since we have shown in the previous sections that the OPLS-AA/AGBNP effective potential with the full nonpolar function [eq. (13)] is suitable for the β-hairpin peptide, we have constructed the potential of mean force of the C-peptide using the same effective potential. The potential of mean force was plotted with respect to the radius of gyration (Rg) of the heavy atoms of the peptide and the helix length. A residue is considered to be in the helical state when its backbone dihedral angles (ϕ and ψ) are $\phi = -60° \pm 30°$ and $\psi = -47° \pm 30°$. The helix length is defined as the number of sequential helical residues, n, minus 3 (i.e., $n - 3$), since four residues are required to make the first turn of the helix. Therefore, the maximum helix length of the C-peptide is 10. We also calculated the helicity fraction of the ensemble of structures. The helicity fraction is defined as

$$\text{helicity fraction} = \frac{\Sigma_i l_i}{\Sigma_i l_{\max}}, \qquad (15)$$

where l_i is the helix length of structure i, $l_{\max}$ is the maximum helix length a structure can have (for the C-peptide, 10), and the sum is over all structures in the generated ensemble. We also analyze the possible salt bridge between residues E2 and R10, since this salt bridge has been observed in the X-ray structure of ribonuclease A[82] and in the NMR spectra of an analogue of the C-peptide.[65] A salt bridge is defined to exist when the distance between O^{ϵ} of E2 and N^{η} of R10 is less than 5.5 Å.

Figure 9 shows the potential of mean force of the C-peptide calculated with the OPLS-AA/AGBNP potential using the full nonpolar function [eq. (13)] and with the standard dielectric screening ($S_i = 1$). (These results are very similar to the results obtained with the surface-area-dependent nonpolar function and standard dielectric screening, which are not shown.) With these parameters, full α-helix formation is not favored. The longest helix observed at 313K is only six residues long, and the helicity fraction of the ensemble of structures is less than 7%. Few structures have a helix length greater than four. This is predominately due to the formation of the salt bridge between E2 and R10 occurring in most of the generated structures. Table I shows the fraction of structures with a particular helical length that possess the E2–R10 salt bridge. For structures with three or fewer sequential α-helical residues (helix length of 0), 79.9% of the structures have this salt bridge. Most of the structures with a helical length between 1 and 4 also have this salt bridge (see Table I). In the X-ray structure of ribonuclease A,[82] the 13-residue N-terminal segment (the C-peptide) possesses the salt bridge between E2 and R10 and has a helix length of four. It is not possible for a helix to span the entire peptide in a structure with the E2–R10 salt bridge. This also has been noted by Osterhout et al. who proposed, based on their NMR experiments on an analogue of the C-peptide, that the ensemble of structures in solution is composed of the following conformations: extended, helical, and partially helical peptides containing the salt bridge between E2 and R10.[65] These observations suggest that disfavoring the formation of salt bridges by the introduction of additional dielectric screening, as we have done in our study of the C-terminal peptide of the B1 domain of protein G, would favor α-helical conformations. We present these results below.

TABLE I. Percentage of Structures of Specified Helix Lengths with Salt Bridges Between E2 and R10

Helix length	Structures with salt bridges (%)	
	$S_i = 1.0$[a]	$S_i = 0.5$[b]
0	79.9	50.9
1	98.5	0.9
2	99.0	0.8
3	98.4	2.3
4	91.5	0.2
5	0.0	0.1
6	0.0	0.0
8	—	0.0
9	—	0.0
10	—	0.0

[a]OPLS-AA/AGBNP with full nonpolar model and default dielectric screening.
[b]OPLS-AA/AGBNP with full nonpolar model and additional dielectric screening of charged side chains.

The potential of mean force obtained using additional dielectric screening ($S_i = 0.5$ for atoms with formal charges) with the OPLS-AA/AGBNP potential is shown in Figure 10. This figure shows that complete helices (i.e., a helix length of 10) are present in the ensemble of structures generated with this potential. The helicity fraction in the ensemble is around 30%, which is in good agreement with the experimental results of the Baldwin group.[33] We see an increase in both the helicity fraction and the helix length due to the additional dielectric screening, which diminishes the propensity toward the formation of the E2–R10 salt bridge. This is clearly evident in Table I, which shows a very large reduction in the percentage of structures with any helical content that possess this salt bridge. A significant number of structures in the nonhelical ensemble (around 50%) contain the E2–R10 salt bridge even in the presence of increased dielectric screening. The salt bridge is absent in structures with a helical length greater than five. Our results contradict previous theoretical studies that used a sigmoidal distance-dependent dielectric to model solvation. In those studies, the lowest energy conformation was a partially helical structure with the salt bridge between E2 and R10.[66,67] It is known that

the solvent model used in their study tends to overestimate the stability of salt bridges.

The range of Rg values we observed (e.g., Fig. 10) was between 5.5 and 7.5 Å. This limited Rg range indicates that the nonhelical structures are in a globular state rather than an extended one. The Rg of the globular state is close to that of the helical structures. The reason for this lies in the fact that many of the residues in the C-peptide sequence have long side chains. The globular nonhelical structures have folded into conformations where the long side chains protrude outwards, resulting in a Rg similar to that of the helix. We observed that, at higher temperatures, the range of Rg values increased to 12 Å, apparently because of the occurrence of extended conformations not energetically stable at lower temperatures. Based on our results, we propose that the structural ensemble of the C-peptide in solution contains the following principal conformations: helical structures and globular nonhelical structures with and without the salt bridge between E2 and R10. Our ensemble agrees with the NMR results of Osterhout et al.[65] in that we observed helical and nonhelical structures. Our results differ in that we did not observe to any significant degree partially helical conformations that had the E2–R10 salt bridge as they proposed; they did not directly observe the presence of the salt bridge. We found that the E2–R10 salt bridge is only significantly present in the globular nonhelical structures of the ensemble.

CONCLUSIONS

We found that the OPLS-AA force field with the AGBNP implicit solvent model correctly predicts the propensity of two peptides toward their corresponding α-helical and β-hairpin conformations in solution. The potential of mean force generated with the OPLS-AA/AGBNP potential for the β-hairpin-forming C-terminal peptide of protein G (see Fig. 6) has features similar to those found for the free energy surfaces generated using explicit solvent models.[46,47] These features include an unfolded region centered around zero native hydrogen bonds and regions of collapsed and folded structures with less than 7 Å Rg of the hydrophobic-core residues. Our results, however, differ in that the generated potential of mean force exhibits a free energy barrier between the unfolded and collapsed regions not found in the explicit solvent results.[46,47] This difference is possibly due to the longer equilibration time we use for the replica exchange simulations reported here (2 ns as compared to ~100 ps[46,47]) prior to collecting data; we observe that the free energy barrier converges later than other features of the potential of mean force.

Key factors in generating the correct potential of mean force for the C-terminal peptide of protein G are the implementation of an improved nonpolar solvation free energy function and increased dielectric screening of charged side chains. The AGBNP nonpolar function favors the formation of the collapsed hydrophobic core of the β-hairpin. The additional dielectric screening of charged side chains that we implemented in the AGBNP model prevents the formation of a salt bridge between K50 and E56, which disrupts β-hairpin formation. But this increased screening is not so severe that it still allows for the formation of the salt bridges between D47 and K50 and between the N- and C-termini. The salt bridge between D47 and K50 helps stabilize the β-hairpin.[49] The β-hairpin population of the zwitterion form of the peptide (40%) is in good agreement with the experimental results of Blanco et al. (42%).[35]

The OPLS-AA/AGBNP potential with added dielectric screening was also found to be effective in reproducing the expected potential of mean force for the C-peptide from ribonuclease A, an α-helical-forming peptide. The helicity fraction of around 30% agrees well with the results of CD measurements.[33] And as indicated by the NMR measurements of Osterhout et al.,[65] we found that the conformational ensemble is composed of both helical conformations and nonhelical conformations with and without a salt bridge between residues E2 and R10.

We found that the correct free energy surfaces for the β-hairpin and α-helix are not obtained with a standard nonpolar free energy term based on surface area alone using a simple surface tension with a low value ($\gamma = 15$ cal/mol/Å^2). The OPLS-AA/AGBNP effective potential with additional dielectric screening of charged side chains will be useful for studying the thermodynamics and kinetics of both α-helix and β-hairpin formation. This effective potential has the right balance between the nonpolar effective potential terms which result in compact structures and the polar and hydrogen bonding terms that are specific to secondary structure formation. The peptides we used in this study are naturally occurring sequences that appear in proteins. The ability to correctly reproduce the α-helix and β-hairpin propensities of native peptides is an important step in the application of the OPLS-AA/AGBNP effective potential to the larger goals of protein homology modeling and simulations of protein folding.

ACKNOWLEDGMENTS

This project has been supported in part by the National Institutes of Health Grant GM-30580 and by the BIOMAPS Institute for Quantitative Biology at Rutgers University.

REFERENCES

1. Eaton WA, Muñoz VM, Hagen SJ, Jas GS, Lapidus LJ, Henry ER, Hofrichter J. Fast kinetics and mechanisms in protein folding. Annu Rev Biophys Biomol Struct 2000;29:327–359.
2. Myers JK, Oas TG. Mechanism of fast protein folding. Annu Rev Biochem 2002;71:783–815.
3. Dinner AR, Šali A, Smith LJ, Dobson CM, Karplus M. Understanding protein folding via free-energy surfaces from theory and experiment. Trends Biochem Sci 2000;25:331–339.
4. Rumbley J, Hoang L, Mayne L, Englander SW. An amino acid code for protein folding. Proc Natl Acad Sci USA 2001;98:105–112.
5. Fersht AR, Daggett V. Protein folding and unfolding at atomic resolution. Cell 2002;108:573–582.
6. Vendruscolo M, Paci E. Protein folding: bringing theory and experiment closer together. Curr Opin Struct Biol 2003;13:82–87.
7. Lazaridis T, Karplus M. Discrimination of the native from misfolded protein models with an energy function including implicit solvation. J Mol Biol 1999;288:477–487.
8. Petrey D, Honig B. Free energy determinants of tertiary structure and the evaluation of protein models. Protein Sci 2000;9:2181–2191.

9. Lazaridis T, Karplus M. Effective energy functions for protein structure prediction. Curr Opin Struct Biol 2000;10:139–145.
10. Bursulaya BD, Brooks III CL. Comparative study of the folding free energy landscape of a three-stranded β-sheet protein with explicit and implicit solvent models. J Phys Chem B 2000;104: 12378–12383.
11. Dominy BN, Brooks III CL. Identifying native-like protein structures using physics-based potentials. J Comput Chem 2002;23:147–160.
12. Liu Y, Beveridge DL. Exploratory studies of *ab initio* protein structure prediction: multiple copy simulated annealing, AMBER energy functions, and a generalized Born/solvent accessibility solvation model. Proteins 2002;46:128–146.
13. Feig M, Brooks III CL. Evaluating CASP4 predictions with physical energy functions. Proteins 2002;49:232–245.
14. Felts AK, Gallicchio E, Wallqvist A, Levy RM. Distinguishing native conformations of proteins from decoys with an effective free energy estimator based on the OPLS all-atom force field and the surface generalized Born solvent model. Proteins 2002;48:404–422.
15. Rhee YM, Pande VS. Multiplexed-replica exchange molecular dynamics method for protein folding simulation. Biophys J 2003; 84:775–786.
16. Dinner AR, Lazaridis T, Karplus M. Understanding β-hairpin formation. Proc Natl Acad Sci USA 1999;96:9068–9073.
17. Zagrovic B, Sorin EJ, Pande V. β-hairpin folding simulations in atomistic detail using an implicit solvent model. J Mol Biol 2001;313:151–169.
18. Zhou R, Berne BJ. Can a continuum solvent model reproduce the free energy landscape of a β-hairpin folding in water? Proc Natl Acad Sci USA 2002;99:12777–12782.
19. Zhou R. Free energy landscape of protein folding in water: explicit vs. implicit solvent. Proteins 2003;53:148–161.
20. Roux B, Simonson T. Implicit solvent models. Biophys Chem 1999;78:1–20.
21. Bashford D, Case DA. Generalized Born models of macromolecular solvation effects. Annu Rev Phys Chem 2000;51:129–152.
22. Simonson T. Macromolecular electrostatics: continuum models and their growing pains. Curr Opin Struct Biol 2001;11:243–252.
23. Zhu J, Shi Y, Liu H. Parameterization of a generalized Born/solvent-accessible surface area model and applications to the simulation of protein dynamics. J Phys Chem B 2002;106:4844–4853.
24. Król M. Comparison of various implicit solvent models in molecular dynamics simulations of immunoglobin G light chain domain. J Comput Chem 2003;24:531–546.
25. Suenaga A. Replica-exchange molecular dynamics simulations for a small-sized protein folding with implicit solvent. J Mol Struct (Theochem) 2003;634:235–241.
26. Gallicchio E, Levy RM. AGBNP, an analytic implicit solvent model suitable for molecular dynamics simulations and high-resolution modeling: method and implementation. J Comput Chem 2003;25: 479–499.
27. Wright PE, Dyson HJ, Lerner RA. Conformation of peptide fragments of proteins in aqueous solution: implications for initiation of protein folding. Biochemistry 1988;27:7167–7175.
28. Epand RM, Scheraga HA. The influence of long-range interactions on the structure of myoglobin. Biochemistry 1968;7:2864–2872.
29. Howard JC, Ali A, Scheraga HA, Momany FA. Investigation of the conformations of four tetrapeptides by nuclear magnetic resonance and circular dichroism spectroscopy, and conformational energy calculations. Macromolecules 1975;8:607–622.
30. Zimm BH, Bragg JK. Theory of the phase transition between helix and random coil in polypeptide chain. J Chem Phys 1959;31:526–535.
31. Lifson S, Roig A. On the theory of helix-coil transition in polypeptide. J Chem Phys 1961;34:1963–1974.
32. Blanco F, Ramírez-Alvarado M, Serrano L. Formation and stability of β-hairpin structures in polypeptides. Curr Opin Struct Biol 1998;8:107–111.
33. Bierzynski A, Kim PS, Baldwin RL. A salt bridge stabilizes the helix formed by isolated C-peptide of RNase A. Proc Natl Acad Sci USA 1982;79:2470–2474.
34. Shoemaker KR, Kim PS, Brems DN, Marqusee S, York EJ, Chaiken IM, Stewart JM, Baldwin RL. Nature of the charged-group effect on the stability of the C-peptide helix. Proc Natl Acad Sci USA 1985;82:2349–2353.
35. Blanco FJ, Rivas G, Serrano L. A short linear peptide that folds into a native stable β-hairpin in aqueous solution. Nature Struct Biol 1994;1:584–590.
36. Blanco FJ, Serrano L. Folding of protein G B1 domain studied by the conformational characterization of fragments comprising its secondary structure elements. Eur J Biochem 1995;230:634–649.
37. Muñoz V, Thompson PA, Hofrichter J, Eaton WA. Folding dynamics and mechanism of β-hairpin formation. Nature 1997;390:196–199.
38. Muñoz V, Henry ER, Hofrichter J, Eaton WA. A statistical mechanical model for β-hairpin kinetics. Proc Natl Acad Sci USA 1998;95:5872–5879.
39. Honda S, Kobayashi N, Munekata E. Thermodynamics of a β-hairpin structure: evidence for cooperative formation of folding nucleus. J Mol Biol 2000;295:269–278.
40. Kobayashi N, Honda S, Yoshii H, Munekata E. Role of side-chains in the cooperative β-hairpin folding of the short C-terminal fragment derived from Streptococcal protein G. Biochemistry 2000;39:6564–6571.
41. Kolinski A, Ilkowski B, Skolnick J. Dynamics and thermodynamics of β-hairpin assembly: insights from various simulation techniques. Biophys J 1999;77:2942–2952.
42. Zhou Y, Linhananta A. Role of hydrophilic and hydrophobic contacts in folding of the second β-hairpin fragment of protein G: molecular dynamics simulation studies of an all-atom model. Proteins 2002;47:154–162.
43. Pande V, Rokhsar DS. Molecular dynamics simulations of unfolding and refolding of a β-hairpin fragment of protein G. Proc Natl Acad Sci USA 1999;96:9062–9067.
44. Roccatano D, Amadei A, Di Nola A, Berendsen HJ. A molecular dynamics study of the 41–56 β-hairpin from B1 domain of protein G. Protein Sci 1999;8:2130–2143.
45. Ma B, Nussinov R. Molecular dynamics simulations of a β-hairpin fragment of protein G: balance between side-chain and backbone forces. J Mol Biol 2000;296:1091–1104.
46. García AE, Sanbonmatsu KY. Exploring the energy landscape of a β-hairpin in explicit solvent. Proteins 2001;42:345–354.
47. Zhou R, Berne BJ, Germain R. The free energy landscape for β-hairpin folding in explicit water. Proc Natl Acad Sci USA 2001;98:14931–14936.
48. Lee J, Shin S. Two-dimensional correlation analysis of peptide unfolding: molecular dynamics simulations of β-hairpins. J Phys Chem B 2002;106:8796–8802.
49. Tsai J, Levitt M. Evidence of turn and salt bridge contributions to β-hairpin stability: MD simulations of C-terminal fragment from the B1 domain of protein G. Biophys Chem 2002;101–102:187–201.
50. Gnanakaran S, Nymeyer H, Portman J, Sanbonmatsu KY, and García AE. Peptide folding simulations. Curr Opin Struct Biol 2003;13:168–174.
51. Sugita Y, Okamoto Y. Replica-exchange molecular dynamics method for protein folding. Chem Phys Lett 1999;314:141–151.
52. Mitsutake A, Sugita Y, Okamoto Y. Generalized-ensemble algorithms for molecular simulations of biopolymers. Biopolymers 2001;60:96–123.
53. Schaefer M, Bartels C, Karplus M. Solution conformations and thermodynamics of structured peptides: molecular dynamics simulation with an implicit solvation model. J Mol Biol 1998;284:835–848.
54. Jorgensen WL, Maxwell DS, Tirado-Rives J. Development and testing of the OPLS all-atom force field on conformational energetics and properties of organic liquids. J Am Chem Soc 1996;118: 11225–11236.
55. Kaminski GA, Friesner RA, Tirado-Rives J, Jorgensen WL. Evaluation and reparameterization of the OPLS-AA force field for proteins via comparison with accurate quantum chemical calculations on peptides. J Phys Chem B 2001;105:6474–6487.
56. Gronenborn AM, Filpula DR, Essig NZ, Achari A, Whitlow M, Wingfield PT, Clore GM. A novel, highly stable fold of the immunoglobulin binding domain of Streptococcal protein G. Science 1991;253:657–661.
57. Bolhuis PG. Transition-path sampling of β-hairpin folding. Proc Natl Acad Sci USA 2003;100:12129–12134.
58. Lazaridis T, Karplus M. Effective energy function for proteins in solution. Proteins 1999;35:133–152.
59. Qiu D, Shenkin PS, Hollinger FP, Still WC. The GB/SA continuum

model for solvation. A fast analytical method for the calculation of approximate Born radii. J Phys Chem A 1997;101:3005–3014.
60. Ghosh A, Rapp CS, Friesner RA. Generalized Born model based on a surface integral formulation. J Phys Chem B 1998;102:10983–10990.
61. Weiner SJ, Kollman PA, Case DA, Singh UC, Ghio C, Alagone G, Profeta S, Weiner P. A new force field for molecular mechanical simulation of nucleic acids and proteins. J Am Chem Soc 1984;106:765–784.
62. Ma B, Nussinov R. Explicit and implicit water simulations of a β-hairpin peptide. Proteins 2000;37:73–87.
63. de Alba E, Rico M, Jiménez MA. Cross-strand side-chain interactions versus turn conformation in β-hairpins. Protein Sci 1997;6:2548–2560.
64. Brown JE, Klee WA. Helix-coil transition of the isolated amino terminus of ribonuclease. Biochemistry 1971;10:470–476.
65. Osterhout, Jr. JJ, Baldwin RL, York EJ, Stewart JM, Dyson HJ, Wright PE. ^{1}H NMR studies of the solution conformations of an analogue of the C-peptide of ribonuclease A. Biochemistry 1989;28:7059–7064.
66. Hansmann UHE, Okamoto Y. Tertiary structure prediction of C-peptide of ribonuclease A by multicanonical algorithm. J Phys Chem B 1998;102:653–656.
67. Hansmann UHE, Okamoto Y. Effects of side-chain charges on α-helix stability in C-peptide of ribonuclease A studied by multicanonical algorithm. J Phys Chem B 1999;103:1595–1604.
68. Kinoshita M, Okamoto Y, Hirata F. Analysis on the conformational stability of C-peptide of ribonuclease A in water using the reference interaction site model theory and Monte Carlo simulated annealing. J Chem Phys 1999;110:4090–4100.
69. Okamoto Y. Tackling the multiple-minima problem in protein folding by Monte Carlo simulated annealing and generalized-ensemble algorithms. Intl J Mod Phys C 1999;10:1571–1582.
70. Mitsutake A, Sugita Y, Okamoto Y. Replica-exchange multicanonical and multicanonical replica-exchange Monte Carlo simulations of peptides. II. Application to a more complex system. J Chem Phys 2003;118:6676–6688.
71. Roccatano D, Colombo G, Fioroni M, Mark AE. Mechanism by which 2,2,2-triflouroethanol/water mixtures stabilize secondary-structure formation in peptides: a molecular dynamics study. Proc Natl Acad Sci USA 2002;99:12179–12184.
72. Levy RM, Zhang LY, Gallicchio E, Felts AK. On the nonpolar hydration free energy of proteins: surface area and continuum solvent models for the solute–solvent interaction energy. J Am Chem Soc 2003;125:9523–9530.
73. Srinivasan J, Trevathan MW, Beroza P, Case DA. Application of a pairwise generalized Born model to proteins and nucleic acids: inclusion of salt effects. Theor Chem Acc 1999;101:426–434.
74. Jacobson MP, Friesner RA, Xiang Z, Honig B. On the role of the crystal environment in determining side-chain conformations. J Mol Biol 2002;320:597–608.
75. Jacobson MP, Pincus DL, Rapp CS, Day TJF, Honig B, Shaw DE, Friesner RA. A hierarchical approach to all-atom protein loop prediction. Proteins 2004;55:351–367.
76. Yu Z, Jacobson MP, Friesner RA. In preparation.
77. Chothia C. Conformation of twisted β-pleated sheets in proteins. J Mol Biol 1973;75:295–302.
78. Chothia C. Coiling of β-pleated sheets. J Mol Biol 1983;163:107–117.
79. Salemme FR. Structural properties of protein β-sheets. Prog Biophys Mol Biol 1983;42:95–133.
80. Maccallum PH, Poet R, Milner-White EJ. Coulombic attractions between partially charged main-chain atoms stabilise the right-handed twist found in most β-strands. J Mol Biol 1995;248:374–384.
81. Scheraga HA, Vila JA, Ripoll DR. Helix-coil transition re-visited. Biophys Chem 2002;101–102:255–265.
82. Tilton Jr RF, Dewan JC, Petsko GA. Effects of temperature on protein structure and dynamics: X-ray crystallographic studies of the protein ribonuclease-A at nine different temperatures from 98 to 320K. Biochemistry 1992;31:2469–2481.